Journal of Materials Science and Chemical Engineering, 2026, 14(1), 15-26
https://www.scirp.org/journal/msce
ISSN Online: 2327-6053
ISSN Print: 2327-6045

Preparation of Eu^{3+}-Doped $Ca_{0.8}Yb_{0.2}F_{2.2}$ as a Fluorescent Probe and Its Application in Detecting CrO_4^{2-} and $Cr_2O_7^{2-}$ Ions

Lexiang Zhou, Lu Lei, Xiao Qu, Shanshan Hu*

School of Chemistry and Chemical Engineering, Southwest University, Chongqing, China
Email: *hushan3@swu.edu.cn

How to cite this paper: Zhou, L.X., Lei, L., Qu, X. and Hu, S.S. (2026) Preparation of Eu^{3+}-Doped $Ca_{0.8}Yb_{0.2}F_{2.2}$ as a Fluorescent Probe and Its Application in Detecting CrO_4^{2-} and $Cr_2O_7^{2-}$ Ions. *Journal of Materials Science and Chemical Engineering*, **14**, 15-26.
https://doi.org/10.4236/msce.2026.141002

Received: December 15, 2025
Accepted: January 13, 2026
Published: January 16, 2026

Abstract

The accurate detection of hexavalent chromium (Cr(VI)) is crucial for environmental protection and public health. Rare earth fluorides have attracted considerable attention as fluorescent sensing materials due to their distinctive properties, including low lattice phonon energy, exceptional chemical stability and long fluorescence lifetime. This study reports the successful one-step hydrothermal synthesis of a Eu^{3+}-doped $Ca_{0.8}Yb_{0.2}F_{2.2}$ fluorescent probe with excellent aqueous dispersibility. The obtained probe showed high sensitivity towards CrO_4^{2-} and $Cr_2O_7^{2-}$ ions, achieving detection limits of 1.45 μM and 1.50 μM. The obtained probe exhibited remarkable stability across a wide pH range (3 - 11) and strong anti-interference capability, confirming its suitability for analyzing real water samples. Owing to its robust performance and straightforward operation, this fluorescent probe presents a promising approach for efficient monitoring of trace Cr(VI) contaminants in aqueous environments.

Keywords

Fluorescent Probe, Rare Earth Fluorides, Cr(VI) Detection

1. Introduction

Chromium (Cr) is a pervasive heavy metal pollutant posing significant risks to ecosystems and human health. In environmental and industrial wastewater contexts, chromium primarily exists in two stable oxidation states: the less toxic trivalent form (Cr(III)) and the highly toxic hexavalent form (Cr(VI)) [1]-[3]. Cr(VI) species, predominantly occurring as oxyanions such as chromate (CrO_4^{2-}), hydrogen chromate ($HCrO_4^-$), and dichromate ($Cr_2O_7^{2-}$) depending on pH, are notably soluble and mobile in water systems [4]-[8]. Recognized for its potent tox-

icity and carcinogenicity, Cr(VI) is classified as a Group 1 human carcinogen by the International Agency for Research on Cancer (IARC) [9] [10]. Human exposure, often through industrial discharges, can lead to severe health issues including dermatological irritation, respiratory impairments, ocular damage, and gastrointestinal disorders. At the molecular level, Cr(VI) induces oxidative stress by interfering with cellular redox processes, promotes DNA adduct formation, and can cause chromosomal aberrations, ultimately increasing cancer risk [11] [12].

Consequently, the effective monitoring and removal of Cr(VI) from drinking water and groundwater sources is imperative, particularly its anionic forms (CrO_4^{2-} and $Cr_2O_7^{2-}$). Regulatory bodies worldwide have established stringent limits; for instance, the U.S. Environmental Protection Agency (EPA) sets a maximum contaminant level (MCL) of 0.1 mg/L for total chromium [13], while Chinese standards (GB 5749-2006) impose a stricter limit of 0.05 mg/L specifically for Cr(VI) [14]. This underscores the urgent need for developing reliable, sensitive, and selective methods for Cr(VI) detection in water.

Conventional techniques for chromium analysis, such as Flame Atomic Absorption Spectrometry (FAAS), Graphite Furnace Atomic Absorption Spectrometry (GFAAS), Inductively Coupled Plasma-based methods (ICP-OES, ICP-MS), and X-ray Fluorescence (XRF), offer precision but often require sophisticated instrumentation, extensive sample preparation, and skilled operation, limiting their field applicability [15]-[17]. In contrast, fluorescence-based sensing has emerged as a powerful alternative due to its inherent advantages of high sensitivity, selectivity, rapid response, and operational simplicity. While numerous fluorescent probes for chromium detection have been explored, and most of them are based on organic fluorophores. Recent efforts have focused on designing novel probes for enhanced Cr(VI) selectivity and sensitivity. For example, Subash *et al.* developed a water-compatible N-aryl carbamate-substituted quinoxaline sensor for Cr(VI) with a quantum yield of 0.26, emitting blue-green fluorescence at 498 nm [18]. Wang *et al.* fabricated a composite film incorporating copper nanoclusters for visual and ratiometric fluorescence detection of Cr(VI) [19]. Narasimhappa *et al.* have reported aggregation-induced emission (AIE)-active probes acting as "turn-off" sensors for Cr(VI) and Fe(III), and naphthalene-functionalized metal-organic frameworks (MOFs) for sensing these ions [20].

However, organic probes frequently suffer from limitations such as potential toxicity, poor photostability, or inadequate water solubility, hindering their practical deployment. Inorganic nanomaterials, particularly those doped with lanthanide ions, offer a compelling solution due to their superior photophysical properties—high quantum yield, long luminescence lifetime, excellent photostability and comparatively low toxicity [21]-[24]. Among these, rare earth fluorides stand out as promising host matrices for fluorescent sensors, benefiting from low phonon energies that minimize non-radiative decay, high chemical stability [25] [26] and relatively straightforward synthesis routes like hydrothermal method that often yields products with good aqueous dispersibility [27] [28].

Herein, we present the hydrothermal synthesis of a Eu^{3+}-doped $Ca_{0.8}Yb_{0.2}F_{2.2}$ fluorescent probe exhibiting excellent water dispersibility. The $Ca_{0.8}Yb_{0.2}F_{2.2}$:21% Eu^{3+} material shown stable luminescence and phase integrity in aqueous solutions from pH = 3 to pH = 11. The probe serves as a highly selective and sensitive fluorescent sensor for CrO_4^{2-} and $Cr_2O_7^{2-}$ ions via a quenching mechanism.

2. Experimental Section

2.1. Materials and Synthesis

Ytterbium oxide (Yb_2O_3, 99.99%), Europium oxide (Eu_2O_3, 99.99%), Calcium chloride ($CaCl_2$, AR), Nitric acid (HNO_3, AR), Hydrochloric acid (HCl, AR), Ammonium fluoride (NH_4F, AR) and Ethanol absolute (C_2H_5OH, AR).

The $Ca_{0.8}Yb_{(0.2-x)}F_{2.2}$:x%$Eu^{3+}$ samples were synthesized hydrothermally. For the representative $Ca_{0.8}Yb_{0.2}F_{2.2}$:21%Eu^{3+} sample, 2 mmol of $CaCl_2$ (dissolved in 1 M solution, 2000 μL) was added to 20 mL of deionized water in a 100 mL beaker. Under vigorous stirring, 0.79 mmol of $Yb(NO_3)_3$ (1 M, 790 μL) and 0.21 mmol of $Eu(NO_3)_3$ (1 M, 210 μL) were added sequentially. The mixture was stirred for 20 minutes to ensure homogeneity. Subsequently, 7 mmol of NH_4F (4 M, 1750 μL) was added dropwise, and stirring continued for another 30 minutes, resulting in a milky white suspension. This suspension was transferred into a 50 mL Teflon-lined stainless-steel autoclave and heated at 180˚C for 12 hours. After natural cooling to room temperature, the resulting product was collected by centrifugation (5000 rpm), washed thoroughly with deionized water and ethanol, and finally dried at 60˚C in a vacuum oven for 6 hours.

2.2. Characterization

Powder X-ray diffraction (PXRD) patterns were acquired using a MSALNDS diffractometer (Beijing Purkinje General Instrument) with Cu Kα radiation (λ = 0.154 nm, 36 kV, 20 mA), scanning from 10˚ to 90˚ (2θ). Morphological characterization and elemental analysis (EDS and mapping) were performed using a Sigma 500/10102 Field Emission Scanning Electron Microscope (Carl Zeiss, Germany). Photoluminescence spectra (excitation and emission) were recorded on an FLS fluorescence spectrometer (Edinburgh Instruments, UK).

3. Results and Discussion

3.1. Morphology, Phase and Luminescence

The phase purity and crystal structure of the synthesized $Ca_{0.8}Yb_{0.2}F_{2.2}$:x%Eu^{3+} powder were confirmed by X-ray diffraction (XRD). As shown in **Figure 1**, all diffraction peaks align perfectly with the reference pattern for $Ca_{0.8}Yb_{0.2}F_{2.2}$ (JCPDS 87-0978), indicating the successful formation of the desired crystalline phase without detectable impurities. Elemental composition and distribution were analyzed using Energy Dispersive X-ray Spectroscopy (EDS). The EDS spectrum (**Figure 2(a)**) confirms the presence of Ca, Yb, F, and Eu elements. Furthermore, elemental mapping (**Figures 2(b)-(f)**) reveals a homogeneous distribution

of all these elements throughout the nanoparticles, providing strong evidence for the successful incorporation of Eu^{3+} ions into the $Ca_{0.8}Yb_{0.2}F_{2.2}$ host lattice.

To optimize the luminescence output, samples with varying Eu^{3+} doping concentrations were synthesized. Under 392 nm excitation, the emission spectra (**Figure 3(a)**) are dominated by the characteristic intra-4f transitions of Eu^{3+} ($^5D_0 \rightarrow {}^7FJ$, J = 1 - 4). The dependence of the integrated emission intensity on Eu^{3+} concentration is plotted in **Figure 3(b)**. The intensity initially increases with doping concentration, reaching a maximum at 21%Eu^{3+}, beyond which the quenching occurs. This phenomenon is attributed to enhanced non-radiative energy transfer between neighboring Eu^{3+} ions at shorter inter-ionic distances, prevalent at higher doping levels. Therefore, the $Ca_{0.8}Yb_{0.2}F_{2.2}$:21%Eu^{3+} sample, exhibiting the strongest luminescence, was selected for all subsequent sensing experiments.

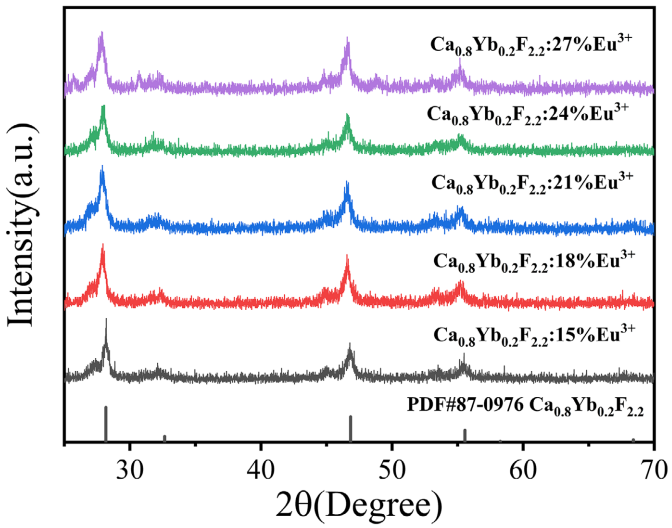

Figure 1. XRD patterns of $Ca_{0.8}Yb_{0.2}F_{2.2}$:x%Eu (x = 15, 18, 21, 24, and 28) phosphors.

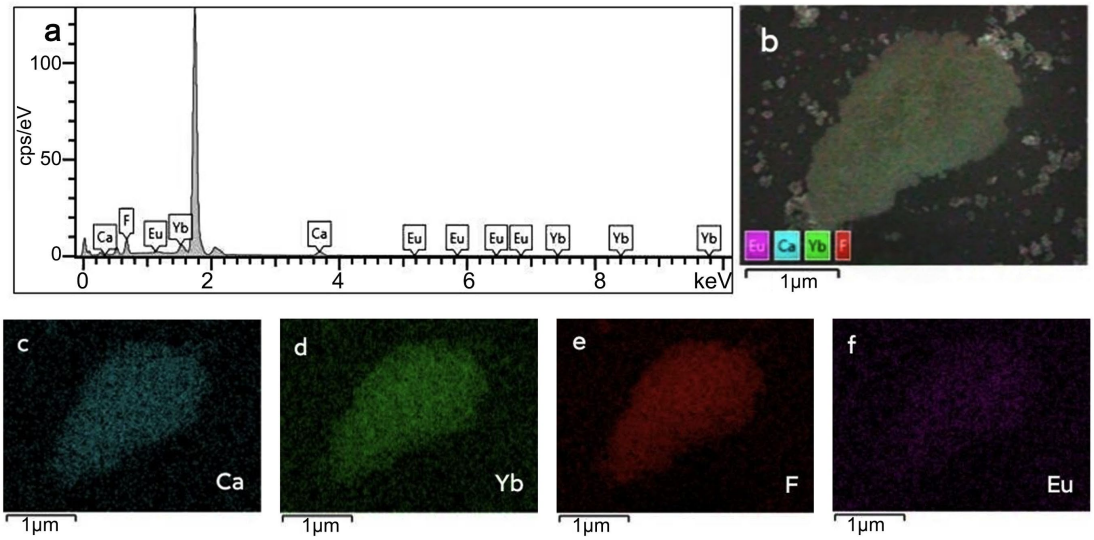

Figure 2. (a) EDS spectrum and (b-f) elemental mapping of $Ca_{0.8}Yb_{0.2}F_{2.2}$:21%Eu^{3+} phosphor.

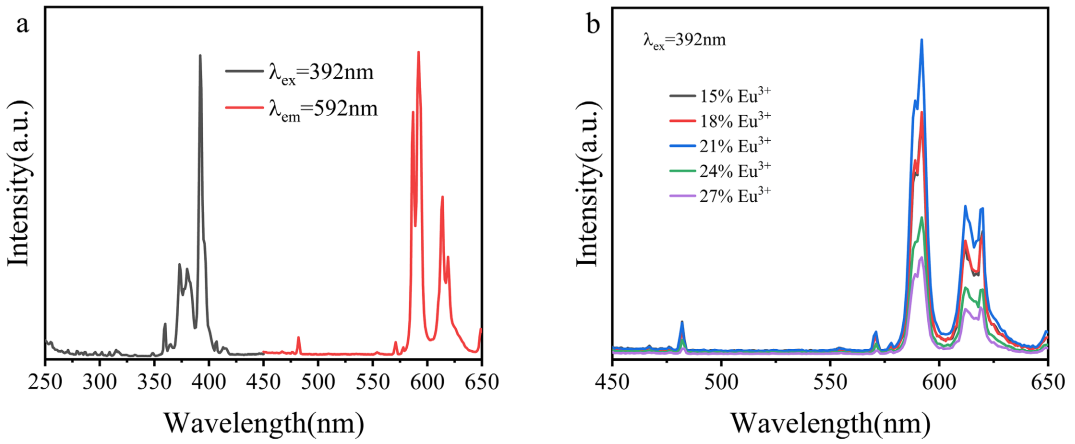

Figure 3. (a) Excitation and emission spectra of $Ca_{0.8}Yb_{0.2}F_{2.2}$:21%Eu^{3+} and (b) Effect of Eu^{3+} concentration on the emission intensity.

3.2. Aqueous Stability and Dispersion

The hydrothermal synthesis method yielded $Ca_{0.8}Yb_{0.2}F_{2.2}$ material with good aqueous dispersibility, which typically improves with lower crystallinity. Furthermore, as a rare-earth fluoride, $Ca_{0.8}Yb_{0.2}F_{2.2}$ maintains excellent chemical stability even at relatively low crystallinity levels. Consequently, the $Ca_{0.8}Yb_{0.2}F_{2.2}$:21%Eu^{3+} powder demonstrates both favorable dispersibility and remarkable pH stability in aqueous environments.

To evaluate the luminescence stability of the $Ca_{0.8}Yb_{0.2}F_{2.2}$:21%Eu^{3+} aqueous suspension, emission spectra were systematically recorded at 20-second intervals. The pH-dependent luminescence behavior was investigated by measuring emission spectra from uniformly mixed suspensions adjusted to different pH values. As shown in **Figure 4(a)**, the luminescence intensity of the $Ca_{0.8}Yb_{0.2}F_{2.2}$:21%Eu^{3+} suspension remained essentially unchanged over a 100-second monitoring period. **Figure 4(b)** demonstrates that the luminescence intensity maintained remarkable consistency across a broad pH range from 3 to 11.

Notably, the crystalline phase of $Ca_{0.8}Yb_{0.2}F_{2.2}$:21%Eu^{3+} powder remained intact after immersion in aqueous solution. The long-term stability assessment (**Figure 5**) revealed excellent retention of luminescence properties, with minimal degradation observed even after 50 days of suspension storage. This combination of phase stability and aqueous dispersibility establishes the fundamental basis for employing $Ca_{0.8}Yb_{0.2}F_{2.2}$:21%Eu^{3+} powder as a reliable sensing platform for analyte detection in aqueous environments [29] [30].

3.3. Selectivity and Sensitivity

The selectivity of the $Ca_{0.8}Yb_{0.2}F_{2.2}$:21%Eu^{3+} probe towards Cr(VI) anions was investigated by monitoring the fluorescence response upon addition of various potential interfering ions, including CO_3^{2-}, F^-, PO_4^{3-}, NO_3^-, SO_4^{2-}, I^-, Br^-, and ClO_3^-. As depicted in **Figure 6(a)**, the introduction of these ions induced negligible changes in the fluorescence intensity compared to the blank suspension. In

stark contrast, the addition of either CrO_4^{2-} or $Cr_2O_7^{2-}$ resulted in significant fluorescence quenching. The histogram in **Figure 6(b)**, representing the emission intensity at 592 nm, clearly visualizes this high selectivity, affirming the probe's specific recognition capability for CrO_4^{2-} and $Cr_2O_7^{2-}$ over other common anions.

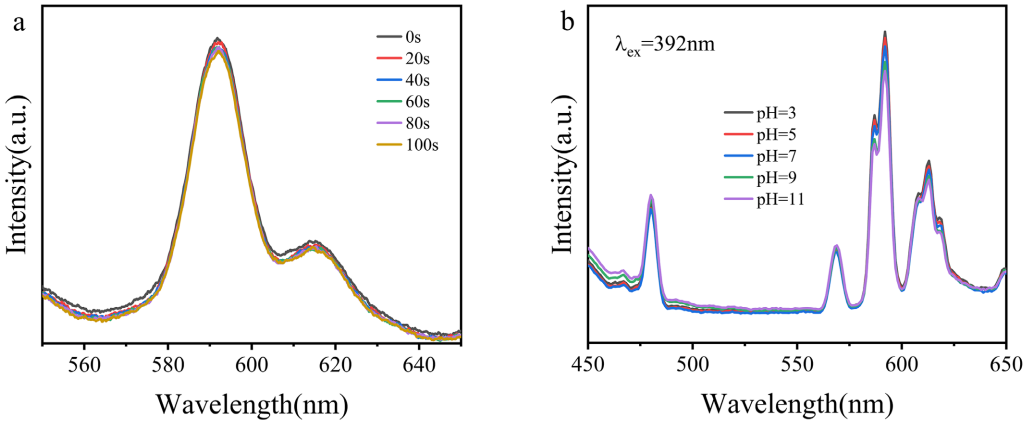

Figure 4. (a) Emission spectra of the aqueous suspension of $Ca_{0.8}Yb_{0.2}F_{2.2}$:21%Eu^{3+} powder recorded at different time intervals; (b) Emission spectra of the suspension at different pH values.

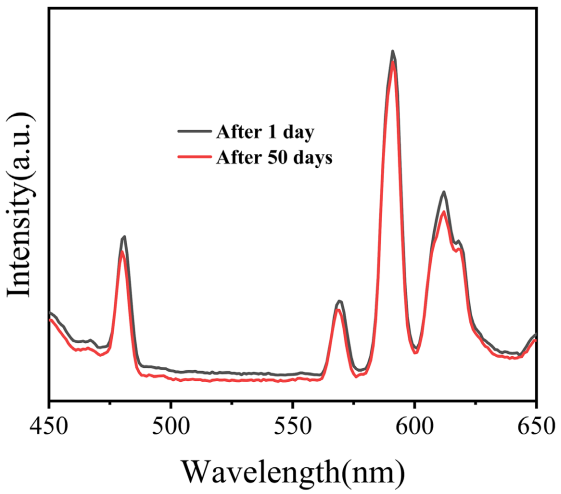

Figure 5. Emission spectra recorded on the 1st day and the 50th day after suspension preparation.

The sensitivity of the probe was quantitatively evaluated by titrating the suspension with increasing concentrations of CrO_4^{2-} and $Cr_2O_7^{2-}$ ions. As shown in **Figure 7(a)** and **Figure 7(b)**, the fluorescence intensity progressively decreased with higher analyte concentrations. The quenching data were analyzed using the Stern-Volmer equation: $I_0/I = 1 + K_{SV}[M]$, where I_0 and I are the fluorescence intensities in the absence and presence of the quencher, respectively, K_{SV} is the Stern-Volmer quenching constant, and [M] is the molar concentration of the quencher. The plots of I_0/I versus quencher concentration ($[CrO_4^{2-}]$ or $[Cr_2O_7^{2-}]$) exhibited good linearity ($R^2 = 1$ for CrO_4^{2-}, $R^2 = 0.996$ for $Cr_2O_7^{2-}$), as shown in

Figure 7(c) and **Figure 7(d)**. The K_{SV} values were determined to be 0.00867 μM^{-1} for CrO_4^{2-} and 0.0084 μM^{-1} for $Cr_2O_7^{2-}$. The limits of detection (LOD), calculated based on LOD = $3\sigma/S$ (where σ is the standard deviation of the blank signal and S is the slope of the calibration curve), were found to be 1.45 μM for CrO_4^{2-} and 1.50 μM for $Cr_2O_7^{2-}$. These LODs values demonstrate the high sensitivity of the probe.

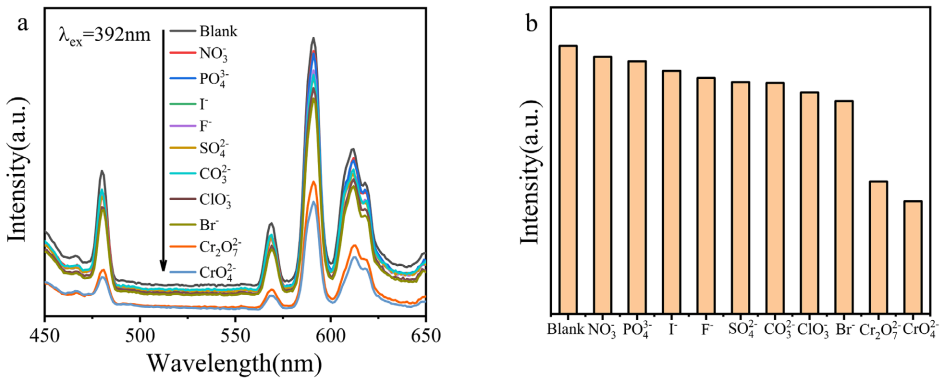

Figure 6. (a) Emission spectra of $Ca_{0.8}Yb_{0.2}F_{2.2}$:21%Eu^{3+} phosphor mixed with different anions (l_{ex} = 392 nm); (b) Comparison of the emission intensity at 592 nm for solutions containing different ions.

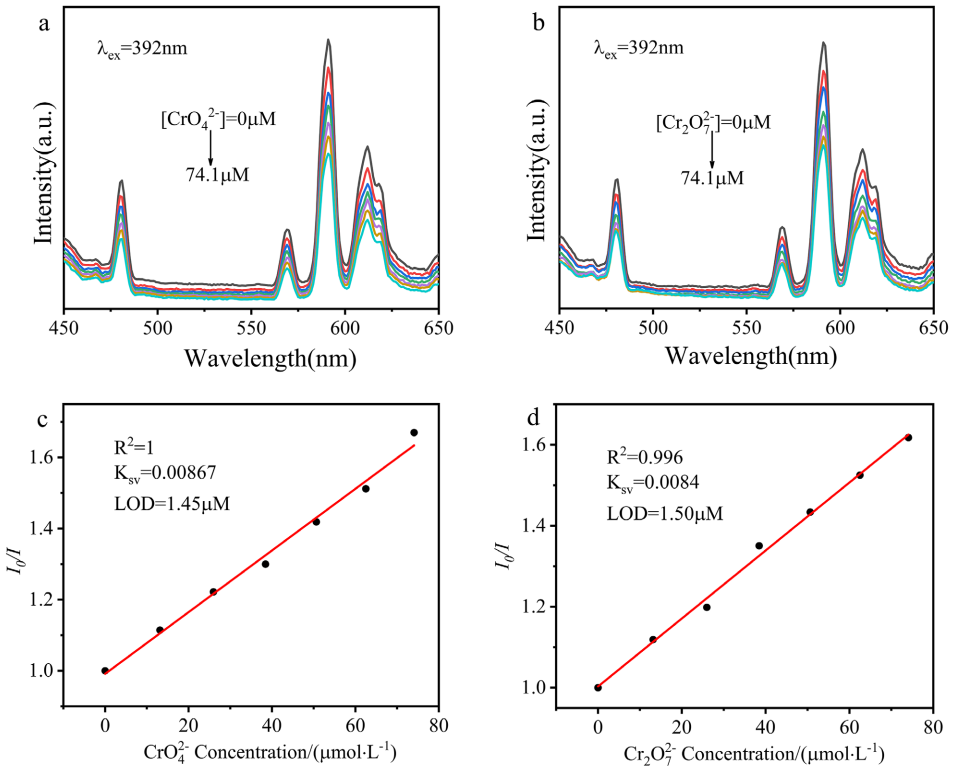

Figure 7. Stern-Volmer plots for the detection of CrO_4^{2-} and $Cr_2O_7^{2-}$ ions using the $Ca_{0.8}Yb_{0.2}F_{2.2}$:21%Eu^{3+} suspension; (a) Emission spectra of the $Ca_{0.8}Yb_{0.2}F_{2.2}$:21%Eu^{3+} suspension at different concentrations of CrO_4^{2-}; (b) Emission spectra of the $Ca_{0.8}Yb_{0.2}F_{2.2}$:21%Eu^{3+} suspension at different concentrations of $Cr_2O_7^{2-}$; (c) Stern-Volmer plot for CrO_4^{2-}; (d) Stern-Volmer plot for $Cr_2O_7^{2-}$.

3.4. Quenching Mechanism

To elucidate the quenching mechanism of $Ca_{0.8}Yb_{0.2}F_{2.2}$:21%Eu^{3+} luminescence by CrO_4^{2-} and $Cr_2O_7^{2-}$ ions, systematic characterization was conducted (**Figure 8**). Phase stability was first investigated by immersing the phosphor in 0.01 mol/L CrO_4^{2-} and $Cr_2O_7^{2-}$ solutions for 24 hours. After centrifugation and drying at 60˚C, XRD patterns revealed that the diffraction peaks of the treated samples remained sharp and closely matched the reference pattern for $Ca_{0.8}Yb_{0.2}F_{2.2}$. This observation confirmed that the crystal structure of $Ca_{0.8}Yb_{0.2}F_{2.2}$:21%Eu^{3+} remained unaltered, thereby ruling out structural alteration of the phosphor as the cause of the luminescence quenching by CrO_4^{2-} and $Cr_2O_7^{2-}$ ions.

UV-Vis absorption spectroscopy revealed that both CrO_4^{2-} and $Cr_2O_7^{2-}$ ions exhibit strong absorption bands in the 200 - 800 nm range (**Figure 9**). This absorption profile significantly overlaps with the excitation spectrum of the $Ca_{0.8}Yb_{0.2}F_{2.2}$:21%Eu^{3+} probe. This spectral overlap suggests that the primary quenching mechanism is the inner filter effect (IFE). The target oxyanions compete with the fluorophore for the excitation light, effectively reducing the number of photons absorbed by the Eu^{3+} ions in the probe, thereby leading to the observed decrease in fluorescence intensity.

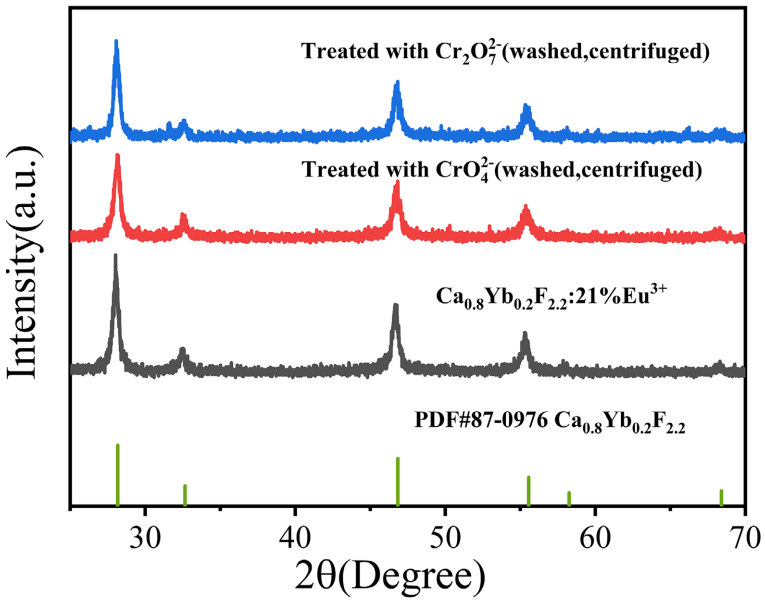

Figure 8. XRD patterns of $Ca_{0.8}Yb_{0.2}F_{2.2}$:21%Eu^{3+} phosphor after immersion in CrO_4^{2-} and $Cr_2O_7^{2-}$ aqueous solutions and subsequent washing/drying.

3.5. Anti-Interference

To assess anti-interference capability, solutions containing CrO_4^{2-} or $Cr_2O_7^{2-}$ were mixed with solutions of potential interfering ions (CO_3^{2-}, F^-, PO_4^{3-}, NO_3^-, SO_4^{2-}, I^-, Br^-, ClO_3^-) at a 1:1 concentration ratio. For the fluorescence measurement, 3 mL of the probe suspension (3 mg/mL) was mixed with 100 μL

of the mixed ion solution (0.01 M for each ion). The fluorescence emission intensity was then measured and compared to that of the blank suspension and the suspension containing only the target Cr(VI) anion. As shown in **Figure 10**, the presence of interfering ions did not significantly alter the pronounced quenching effect caused by CrO_4^{2-} or $Cr_2O_7^{2-}$, confirming the high selectivity of the probe for practical applications.

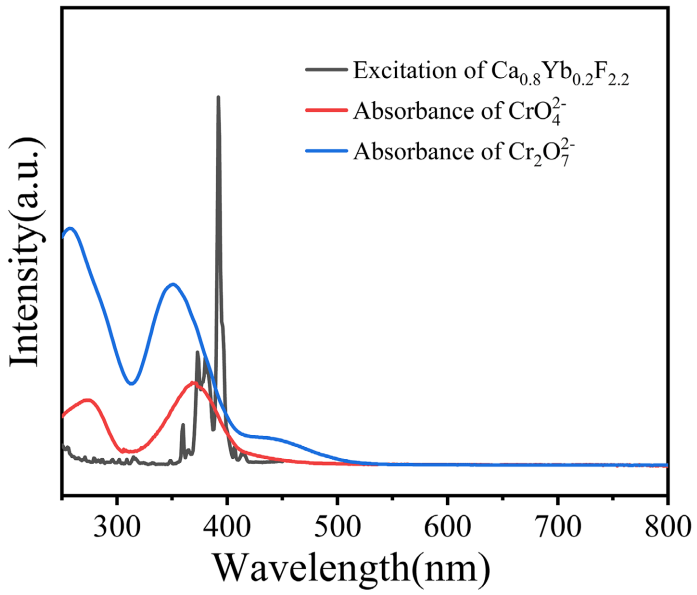

Figure 9. UV-Vis Absorption Spectra of CrO_4^{2-} and $Cr_2O_7^{2-}$ Ions and the excitation spectrum of the $Ca_{0.8}Yb_{0.2}F_{2.2}$:Eu^{3+} phosphor

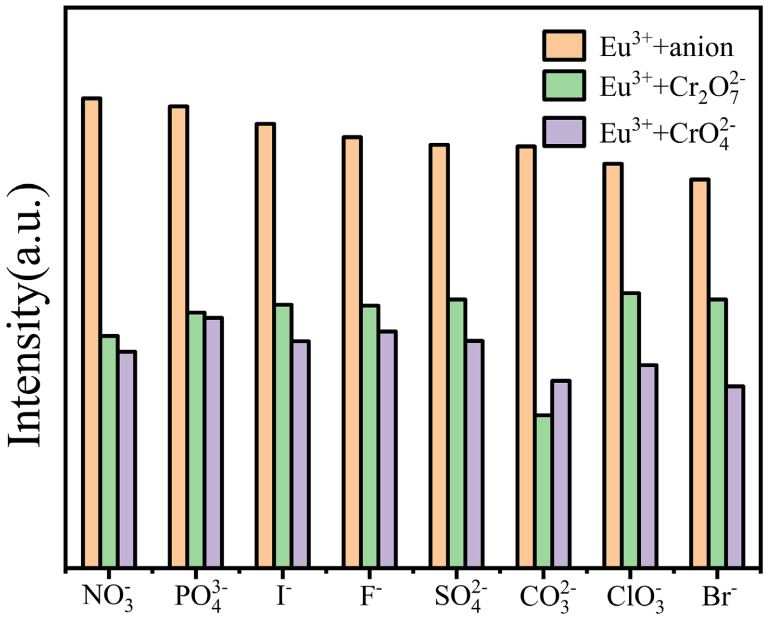

Figure 10. Relative luminescence intensity of the $Ca_{0.8}Yb_{0.2}F_{2.2}$:21%Eu^{3+} suspension after addition of target and interfering ions.

4. Conclusion

In summary, a highly water-dispersible Eu^{3+}-doped $Ca_{0.8}Yb_{0.2}F_{2.2}$ fluorescent probe was successfully synthesized via a facile one-step hydrothermal method. The optimal luminescence intensity was achieved with a Eu^{3+} doping concentration of 21%. The probe serves as a selective sensor for toxic Cr(VI) oxyanions (CrO_4^{2-} and $Cr_2O_7^{2-}$) in water, operating primarily through an inner filter effect mechanism where the analytes compete for excitation energy. It demonstrates high sensitivity, with detection limits of 1.45 μM and 1.50 μM for CrO_4^{2-} and $Cr_2O_7^{2-}$, respectively, values that are significantly lower than the regulatory limit for drinking water. The material exhibits exceptional long-term stability in water and maintains its performance over a wide pH range (3 - 11) with excellent selectivity against common interfering ions. Combined with its simple synthesis and straightforward operation, the $Ca_{0.8}Yb_{0.2}F_{2.2}$:21% Eu^{3+} fluorescent probe represents a reliable and effective tool for the on-site monitoring of trace-level Cr(VI) contamination in real water samples. Furthermore, the design strategy presented here offers valuable insights for developing advanced sensing materials targeting other hazardous heavy metal ions.

Fund

This project was financially sponsored the Natural Science Foundation of Chongqing (cstc2020jcyj-msxmX0332).

Conflicts of Interest

The authors assert that there are no conflicts of interest about the publishing of this work.

References

[1] Huang, F., Li, X., Zhang, Z., Jiang, Z., Wang, G., Li, L. and Yu, Y. (2022) An Ultrastable Eu^{3+} Doped Yttrium Coordination Polymer with Dual-Function Sensing for Cr(VI) and Fe(III) Ions in Aqueous Solution. *Chinese Journal of Structural Chemistry*, **41**, 2204068-2204074.

[2] Liu, S., Zhang, L., Kim, H., Sun, J. and Yoon, J. (2024) Recent Advances and Challenges in Monitoring Chromium Ions Using Fluorescent Probes. *Coordination Chemistry Reviews*, **501**, Article 215575. https://doi.org/10.1016/j.ccr.2023.215575

[3] Khalfaoui, A., Benalia, A., Selama, Z., Hammoud, A., Derbal, K., Panico, A., *et al.* (2024) Removal of Chromium (VI) from Water Using Orange Peel as the Biosorbent: Experimental, Modeling, and Kinetic Studies on Adsorption Isotherms and Chemical Structure. *Water*, **16**, Article 742. https://doi.org/10.3390/w16050742

[4] Hossini, H., Shafie, B., Niri, A.D., Nazari, M., Esfahlan, A.J., Ahmadpour, M., *et al.* (2022) A Comprehensive Review on Human Health Effects of Chromium: Insights on Induced Toxicity. *Environmental Science and Pollution Research*, **29**, 70686-70705. https://doi.org/10.1007/s11356-022-22705-6

[5] Oleksii, Y.A., Mariichak, O.Y., Rozantsev, G.M., Shyshkanov, S.A. and Radio, S.V. (2021) Equilibria Processes in Aqueous Solutions of K_2CrO_4-HNO_3-KNO_3-H_2O and

$K_2Cr_2O_7$-NaOH-KNO_3-H_2O Systems. *Odesa National University Herald. Chemistry*, **26**, 56-72. https://doi.org/10.18524/2304-0947.2021.2(78).233833

[6] Zhu, C., Wang, Q., Huang, X., Li, T. and Yang, G. (2021) Microscopic Understanding about Adsorption and Transport of Different Cr(VI) Species at Mineral Interfaces. *Journal of Hazardous Materials*, **414**, Article 125485. https://doi.org/10.1016/j.jhazmat.2021.125485

[7] Murthy, M.K., Khandayataray, P., Padhiary, S. and Samal, D. (2022) A Review on Chromium Health Hazards and Molecular Mechanism of Chromium Bioremediation. *Reviews on Environmental Health*, **38**, 461-478. https://doi.org/10.1515/reveh-2021-0139

[8] Sharma, P., Singh, S.P., Parakh, S.K. and Tong, Y.W. (2022) Health Hazards of Hexavalent Chromium (Cr (VI)) and Its Microbial Reduction. *Bioengineered*, **13**, 4923-4938. https://doi.org/10.1080/21655979.2022.2037273

[9] Sijko, M., Janasik, B., Wąsowicz, W. and Kozłowska, L. (2021) Can the Effects of Chromium Compounds Exposure Be Modulated by Vitamins and Microelements? *International Journal of Occupational Medicine and Environmental Health*, **34**, 461-490. https://doi.org/10.13075/ijomeh.1896.01706

[10] Meaza, I., Williams, A.R., Wise, S.S., Lu, H. and Wise, J.P. (2024) Carcinogenic Mechanisms of Hexavalent Chromium: From DNA Breaks to Chromosome Instability and Neoplastic Transformation. *Current Environmental Health Reports*, **11**, 484-546. https://doi.org/10.1007/s40572-024-00460-9

[11] Wang, P., Liu, Z., Sweef, O., Saeed, A.F., Kluz, T., Costa, M., *et al.* (2024) Hexavalent Chromium Exposure Activates the Non-Canonical Nuclear Factor Kappa B Pathway to Promote Immune Checkpoint Protein Programmed Death-Ligand 1 Expression and Lung Carcinogenesis. *Cancer Letters*, **589**, 216827. https://doi.org/10.1016/j.canlet.2024.216827

[12] Anjum, A., Mazari, S.A., Hashmi, Z., Jatoi, A.S., Abro, R., Bhutto, A.W., *et al.* (2023) A Review of Novel Green Adsorbents as a Sustainable Alternative for the Remediation of Chromium (VI) from Water Environments. *Heliyon*, **9**, e15575. https://doi.org/10.1016/j.heliyon.2023.e15575

[13] Najm, I. (2025) National Cost of Compliance with a Drinking Water MCL for Hexavalent Chromium. *AWWA Water Science*, **7**, e70035. https://doi.org/10.1002/aws2.70035

[14] Li, H.X., Wu, F.C., Chen, Y.Q., *et al.* (2012) Comparative Analysis on Chinese Water Quality Standards and Foreign Water Quality Standards/Criteria. *China Water & Wastewater*, **28**, 15-18.

[15] Algethami, J.S. (2022) A Review on Recent Progress in Organic Fluorimetric and Colorimetric Chemosensors for the Detection of $Cr^{3+/6+}$ Ions. *Critical Reviews in Analytical Chemistry*, **54**, 487-507. https://doi.org/10.1080/10408347.2022.2082242

[16] Dawra, N. and Dabas, N. (2022) Advances in Spectrophotometric Determination of Chromium(III) and Chromium(VI) in Water: A Review. *International Journal of Environmental Analytical Chemistry*, **104**, 2994-3015. https://doi.org/10.1080/03067319.2022.2076224

[17] Singh, S., Kumar Naik, T.S.S., Chauhan, V., Shehata, N., Kaur, H., Dhanjal, D.S., *et al.* (2022) Ecological Effects, Remediation, Distribution, and Sensing Techniques of Chromium. *Chemosphere*, **307**, Article 135804. https://doi.org/10.1016/j.chemosphere.2022.135804

[18] Subash, J., Mandal, S., Kumar, C.M.V., Sathvika, S., Karthick, V., Pal, S., *et al.* (2025) Investigation of Inventive Quinoxaline-Based Fluorescent Probe for Detection of

Harmful Chromium (VI) Present in Water and Its Bioapplications. *Journal of Environmental Chemical Engineering*, **13**, Article 117068. https://doi.org/10.1016/j.jece.2025.117068

[19] Wang, M., Wu, Y., Liang, Y., Wang, L., Hou, H., Zhang, Z., *et al.* (2024) Copper Nanoclusters Combined with Polymer Films as Highly Sensitive Colorimetric Probes for Visual and Proportional Fluorescence Detection of Hexavalent Chromium Ions in Ph and Natural Waters. *Colloids and Surfaces A*: *Physicochemical and Engineering Aspects*, **702**, Article 135126. https://doi.org/10.1016/j.colsurfa.2024.135126

[20] Narasimhappa, P. and Ramamurthy, P.C. (2025) Modulating Fluorescence Using Naphthalene-Incorporated Tricarboxylate Metal-Organic Framework for Sensing of Chromium and Ferric Ions. *Nanotechnology for Environmental Engineering*, **10**, Article No. 51. https://doi.org/10.1007/s41204-025-00455-3

[21] Wu, H.Y., Yang, J. and Hu, S.S. (2023) Hydrothermal Preparation and Temperature-Sensitive Properties of Sr_2LuF_7:Ln^{3+} (Ln=Yb, Er, Ho) Phosphor. *Journal of Liaocheng University* (*Natural Science Edition*), **146**, 35-42.

[22] Du, H.M., Yang, J. and Hu, S.S. (2023) Upconversion Luminescence and Temperature Sensing Properties of Yb^{3+}/Ho^{3+} Co-Doped $Sc_2W_3O_{12}$ Phosphors. *Journal of Liaocheng University* (*Natural Science Edition*), **152**, 42-49.

[23] Wei, D.L., Yang, X.F., Liu, Y.S., *et al.* (2023) Eu^{3+} Activated Fluoro-Molybdate Red-Emitting Phosphor and Its Luminescent Properties. *Journal of Liaocheng University* (*Natural Science Edition*), **36**, 71-78.

[24] Zhang, X.X., Wang, S.Y., Fu, Q.C., *et al.* (2023) Preparation and Luminescent Properties Regulation of Eu^{3+}-Activated Yellow-Orange Emitting Phosphors. *Journal of Liaocheng University* (*Natural Science Edition*), **36**, 75-85.

[25] Li, J. and Bai, X. (2024) Preparation and Optical Properties of Rare Earth Fluoride and Its Related Composite Materials. *Materials Express*, **14**, 714-720. https://doi.org/10.1166/mex.2024.2671

[26] Wang, Z.Y., Wang, D.M., Hu, S.S., *et al.* (2023) Hydrothermal Synthesis of SrF_2:Tb^{3+} for Selective Detective of Fe^{3+} Ions. *Journal of Liaocheng University* (*Natural Science Edition*), **150**, 35-40.

[27] Deng, E., Zhang, S., Zhu, H., Li, J., Wang, X., Zhang, Y., *et al.* (2025) Facile Hydrothermal Synthesis of Hydroxyapatite Nanosheets as Highly "Active" Supports for Stabilizing Silver Nanoparticles in Toluene Oxidation. *Applied Catalysis A*: *General*, **705**, Article 120438. https://doi.org/10.1016/j.apcata.2025.120438

[28] Yang, J., Jiang, Y., Yang, J., *et al.* (2023) Preparation of $LiLu(MoO_4)_2$: Eu^{3+} and Its Fluorescence Detective for Fe^{3+} Ions. *Journal of Liaocheng University* (*Natural Science Edition*), **37**, 64-69, 88.

[29] Zheng, X., Ren, S., Wang, L., Gai, Q., Dong, Q. and Liu, W. (2021) Controllable Functionalization of Carbon Dots as Fluorescent Sensors for Independent Cr(VI), Fe(III) and Cu(II) Ions Detection. *Journal of Photochemistry and Photobiology A*: *Chemistry*, **417**, Article 113359. https://doi.org/10.1016/j.jphotochem.2021.113359

[30] Lu, H., Wang, Y., Ma, J., Hou, H., He, M., Chen, Q., *et al.* (2026) A Cationic Lanthanide-Based Fluorescent Sensor for Highly Selective and On-Site Detection of Chromium Oxyanions. *Dyes and Pigments*, **246**, Article 113414. https://doi.org/10.1016/j.dyepig.2025.113414